Article

Is metal artefact reduction mandatory in cardiac PET/CT imaging in the presence of pacemaker and implantable cardioverter defibrillator leads?

GHAFARIAN, Pardis, *et al*.

Abstract

Cardiac PET/CT imaging is often performed in patients with pacemakers and implantable cardioverter defibrillator (ICD) leads. However, metallic implants usually produce artefacts on CT images which might propagate to CT-based attenuation-corrected (CTAC) PET images. The impact of metal artefact reduction (MAR) for CTAC of cardiac PET/CT images in the presence of pacemaker, ICD and ECG leads was investigated using both qualitative and quantitative analysis in phantom and clinical studies.

Reference

GHAFARIAN, Pardis, *et al*. Is metal artefact reduction mandatory in cardiac PET/CT imaging in the presence of pacemaker and implantable cardioverter defibrillator leads? *European journal of nuclear medicine and molecular imaging*, 2011, vol. 38, no. 2, p. 252-62

DOI : 10.1007/s00259-010-1635-6
PMID : 20959974

Eur J Nucl Med Mol Imaging (2011) 38:252–262
DOI 10.1007/s00259-010-1635-6

ORIGINAL ARTICLE

Is metal artefact reduction mandatory in cardiac PET/CT imaging in the presence of pacemaker and implantable cardioverter defibrillator leads?

Pardis Ghafarian · S. M. R. Aghamiri · Mohammad R. Ay · Arman Rahmim · Thomas H. Schindler · Osman Ratib · Habib Zaidi

Received: 13 July 2010 / Accepted: 28 September 2010 / Published online: 20 October 2010

Abstract
Purpose Cardiac PET/CT imaging is often performed in patients with pacemakers and implantable cardioverter defibrillator (ICD) leads. However, metallic implants usually produce artefacts on CT images which might propagate to CT-based attenuation-corrected (CTAC) PET images. The impact of metal artefact reduction (MAR) for CTAC of cardiac PET/CT images in the presence of pacemaker, ICD and ECG leads was investigated using both qualitative and quantitative analysis in phantom and clinical studies.
Methods The study included 14 patients with various leads undergoing perfusion and viability examinations using dedicated cardiac PET/CT protocols. The PET data were corrected for attenuation using both artefactual CT images and CT images corrected using the MAR algorithm. The severity and magnitude of metallic artefacts arising from these leads were assessed on both linear attenuation coefficient maps (μ-maps) and attenuation-corrected PET images. CT and PET emission data were obtained using an anthropomorphic thorax phantom and a dedicated heart phantom made in-house incorporating pacemaker and ICD leads attached at the right ventricle of the heart. Volume of interest-based analysis and regression plots were performed for regions related to the lead locations. Bull's eye view analysis was also performed on PET images corrected for attenuation with and without the MAR algorithm.
Results In clinical studies, the visual assessment of PET images by experienced physicians and quantitative analysis did not reveal erroneous interpretation of the tracer distribution or significant differences when PET images were corrected for attenuation with and without MAR. In phantom studies, the mean differences between tracer

P. Ghafarian · S. M. R. Aghamiri (✉)
Department of Radiation Medicine, Shahid Beheshti University,
Tehran, Iran
e-mail: SMR-Aghamiri@cc.sbu.ac.ir

P. Ghafarian · O. Ratib · H. Zaidi
Division of Nuclear Medicine, Geneva University Hospital,
CH-1211 Geneva 4, Switzerland

H. Zaidi
e-mail: habib.zaidi@hcuge.ch

P. Ghafarian · M. R. Ay
Research Center for Science and Technology in Medicine,
Tehran University of Medical Sciences,
Tehran, Iran

M. R. Ay
Department of Medical Physics and Biomedical Engineering,
Tehran University of Medical Sciences,
Tehran, Iran

M. R. Ay
Research Institute for Nuclear Medicine,
Tehran University of Medical Sciences,
Tehran, Iran

A. Rahmim
Department of Radiology, Johns Hopkins University,
Baltimore, MD, USA

T. H. Schindler
Cardiovascular Center, Nuclear Cardiology, Geneva University,
Geneva, Switzerland

H. Zaidi
Geneva Neuroscience Center, Geneva University,
Geneva, Switzerland

uptake obtained without and with MAR were 10.16±2.1% and 6.86±2.1% in the segments of the heart in the vicinity of metallic ICD or pacemaker leads, and were 4.43±0.5% and 2.98±0.5% in segments far from the leads.
Conclusion Although the MAR algorithm was able to effectively improve the quality of μ-maps, its clinical impact on the interpretation of PET images was not significant. Therefore cardiac PET images corrected for attenuation using CTAC in the presence of metallic leads can be interpreted without correction for metal artefacts. It should however be emphasized that in some special cases with multiple ICD leads attached to the myocardium wall, MAR might be useful for accurate attenuation correction.

Keywords Cardiac PET/CT · Metallic artefacts · Metal artefact reduction · Attenuation correction · Pacemaker

Introduction

Myocardial perfusion and viability are increasingly being investigated using PET/CT technology. The advantage of hybrid PET/CT scanners over stand-alone PET is their ability to provide combined morphological and functional data in a "one-stop-shop". In addition, CT images are acquired in a short time in comparison with transmission scanning and provide considerably less noisy attenuation maps (μ-maps) for attenuation correction of the PET images [1, 2]. With the advent of 64-slice and over CT subsystems combined with dedicated PET scanners, full clinical cardiac protocols are now possible including CT angiography and calcium score imaging as an adjunct to myocardial viability and perfusion imaging using dedicated radiotracers. Beyond the vast potential of combined cardiac anatomical and functional imaging on combined PET/CT scanners [3], PET data can be corrected for photon attenuation using corresponding CT images. However, CT images may exhibit streak artefacts if high-density materials such as metals [4, 5] and oral and intravenous contrast agents [6, 7] were present resulting in erroneous interpretation of both viability and perfusion PET images in those cases with severe artefact. Therefore, the use of CT data for attenuation correction can introduce artefacts into the corrected PET images if metallic artefacts are present, and this might influence the interpretation of the PET images [8, 9]. Such artefacts introduced into the PET images usually result in either over- or underestimation of tracer uptake in some regions [7, 10, 11] and caution is therefore required during CT-based attenuation correction (CTAC) procedures. In addition, the time between PET and CT data acquisition can introduce substantial misalignment owing to different breathing patterns between the two scans so that artefacts and substantial quantification bias might be observed in some segments of the myocardial wall on attenuation-corrected PET images [12–15].

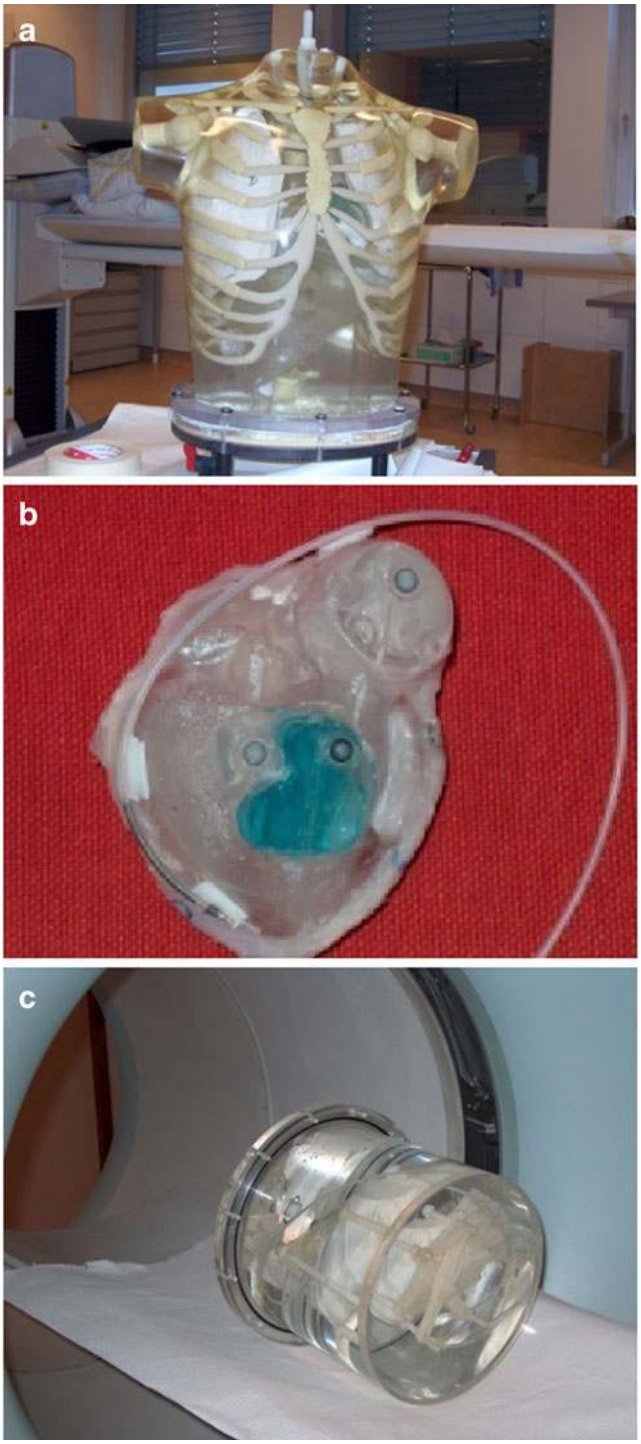

Fig. 1 Photographs of the phantoms used in this study showing: **a** the RSD phantom, **b** the heart model of the RSD phantom with ICD leads attached, **c** heart suspended in a cylindrical water phantom

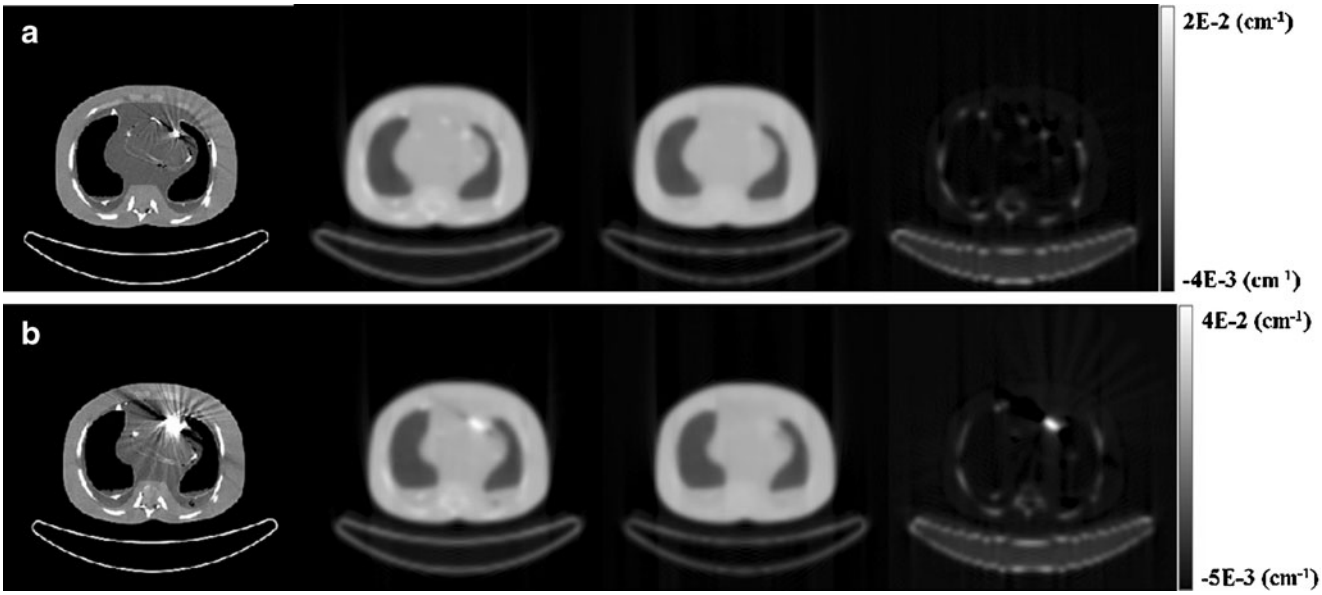

Fig. 2 Metallic artefacts in the heart region of the RSD phantom produced by (**a**) a pacemaker lead and (**b**) an ICD lead. *From left to right*: original CT images, μ-maps generated without MAR, μ-maps generated with MAR, and difference images between μ-maps

In cardiac PET/CT imaging, metallic artefacts may arise owing to the presence of pacemakers and implantable cardioverter defibrillator (ICD) leads. There are different types of pacing and ICD leads located in various regions of the atria and ventricles depending on the cardiac arrhythmic disease. In some patients with ICD leads shock coils may be located in the right ventricle and the superior vena cava. Furthermore, in some patients more than one lead or a combination of pacing and ICD leads might be used.

Various metal artefact reduction (MAR) algorithms have been proposed in the literature [1]. Overall, MAR algorithms can be classified into sinogram-based [11, 16, 17] and image-based [18–20] methods. Metallic artefacts on CT images induce not only anomalous CT numbers but also erode the energy mapping algorithm used for mapping of CT numbers at x-ray energies to attenuation coefficients at 511 keV. DiFilippo and Brunken [5] reported that the increased uptake at the location of ICD electrodes was more pronounced than at the location of pacemaker electrodes. Hamill et al. [18] introduced an image-based MAR algorithm for cardiac PET imaging applications. This algorithm is implemented on commercial software provided on the Biograph TP 64 scanner (Syngo software, Siemens Medical Solutions, Erlangen, Germany).

Table 1 Mean relative differences in linear attenuation coefficients from μ-maps and activity concentrations from PET images between images obtained with and without MAR. PET images obtained with and without MAR were also compared with the actual activity in the phantom (bias). The data were classified according to two artefactual regions including white and black areas

Phantom	Lead	Mean relative difference between images reconstructed without and with MAR				Mean relative difference (bias) between actual and measured activity without and with MAR			
		μ-map		PET		PET without MAR		PET with MAR	
		White region	Black region	White region	Black region	White region	Black region	White region	Black region
Heart	ICD	26.43±1.5 ($p<0.001$)	−7.97±2.0 ($p<0.001$)	11.00±3.3 ($p\leq0.001$)	−5.44±1.0 ($p<0.005$)	−16.46±9.0 ($p<0.01$)	12.40±4.9 ($p<0.05$)	11.58±9.8 ($p<0.05$)	7.67±4.6 ($p=0.065$)
	Pacemaker	18.94±2.0 ($p<0.005$)	−4.42±0.9 ($p<0.001$)	8.35±1.7 ($p<0.001$)	−2.95±0.3 ($p<0.001$)	−8.91±4.8 ($p=0.058$)	−16.23±8.7 ($p=0.141$)	14.38±4.9 ($p<0.005$)	−19.94±9.4 ($p<0.111$)
RSD	ICD	16.43±1.2 ($p<0.001$)	−5.37±1.3 ($p<0.001$)	11.25±2.2 ($p<0.001$)	−7.34±1.9 ($p<0.005$)	−13.21±9.3 ($p<0.001$)	8.32±2.9 ($p<0.05$)	15.38±8.7 ($p<0.05$)	9.67±5.6 ($p=0.053$)
	Pacemaker	16.60±1.3 ($p<0.001$)	−4.10±1.6 ($p<0.001$)	11.94±3.4 ($p<0.001$)	−1.90±0.9 ($p=0.032$)	−11.16±14.0 ($p=0.006$)	−5.14±3.2 ($p=0.358$)	5.76±2.5 ($p=0.619$)	−7.08±4.5 ($p=0.199$)

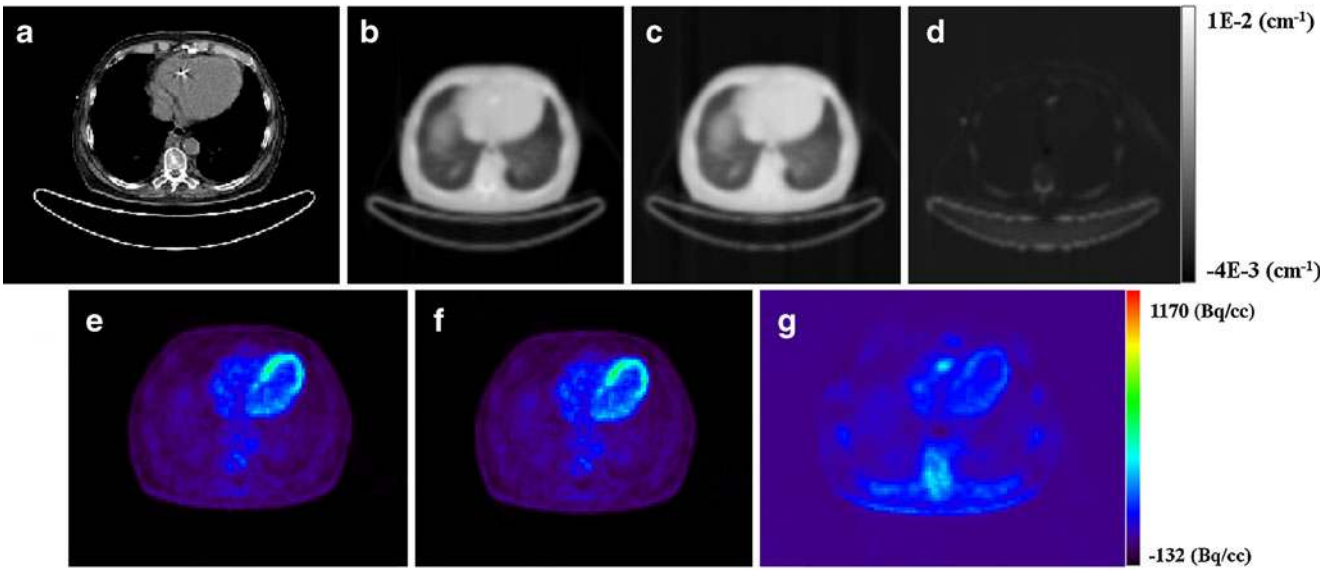

Fig. 3 Typical transverse slice in a patient with a pacemaker lead: **a** original CT image, **b** μ-map generated without MAR, **c** μ-map generated with MAR, **d** difference image between μ-maps, **e** PET image reconstructed without MAR, **f** PET image reconstructed with MAR, **g** difference between PET images

The magnitude and extent of metallic electrode artefacts arising from pacemakers, ICD and ECG leads were investigated on both μ-maps and attenuation-corrected PET images in experimental phantom and clinical studies. Moreover, the performance of the image-based MAR algorithm proposed by Hamill et al. [18] was evaluated with the aim of evaluating the relevance of MAR when using CTAC in cardiac PET imaging and its impact on image interpretation and quantification.

Materials and methods

PET/CT scanner

PET/CT imaging was performed on a Biograph TP 64 scanner (Siemens Medical Solutions, Erlangen, Germany) which offers the ability to perform molecular cardiovascular imaging with the option of using volumetric CT to visualize the anatomy of the coronary arteries. The PET subsystem

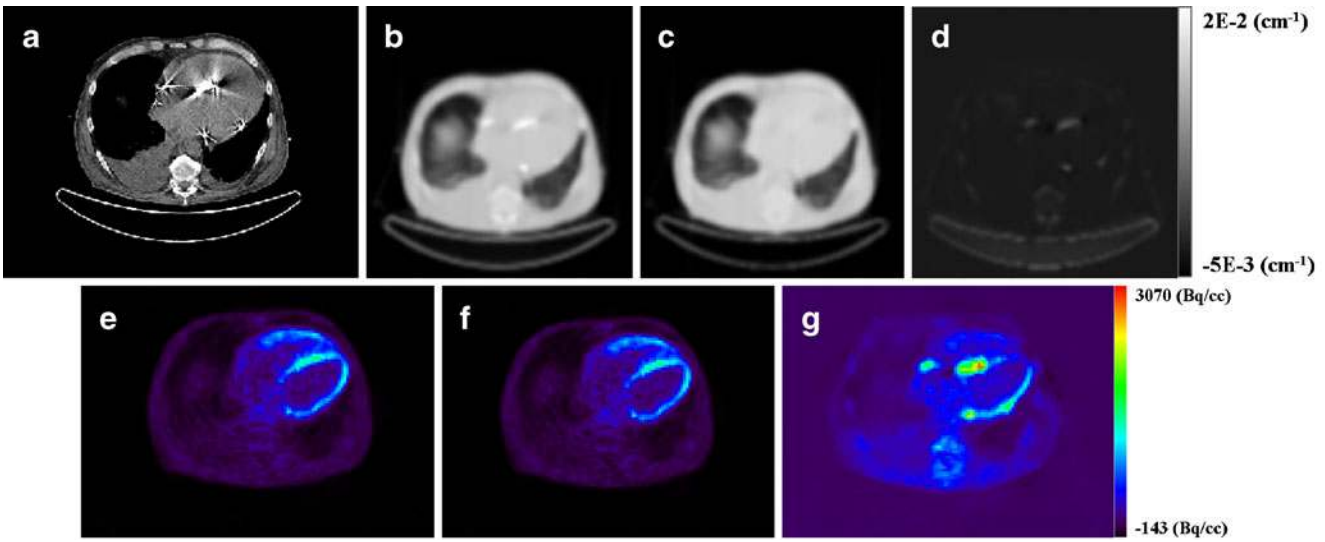

Fig. 4 Typical transverse slice in a patient with an ICD lead: **a** original CT image, **b** μ-map generated without MAR, **c** μ-map generated with MAR, **d** difference image between μ-maps, **e** PET image reconstructed without MAR, **f** PET image reconstructed with MAR, **g** difference between PET images

Table 2 Mean relative difference in tracer uptake in the myocardial wall between PET images corrected for attenuation without and with MAR in patients with ICD and pacemaker leads

Myocardial wall	ICD leads	Pacemaker leads
Anteroseptal	0.76±0.5 (p=1.000)	0.44±0.1 (p=1.000)
Anterolateral	0.75±0.4 (p=0.465)	0.64±0.2 (p=0.102)
Lateroanterior	2.00±1.2 (p=0.351)	1.60±0.5 (p=0.076)
Lateroinferior	2.30±1.2 (p=0.211)	0.60±0.3 (p=0.076)
Inferolateral	2.29±2.1 (p=0.606)	0.57±0.3 (p=0.611)
Inferoseptal	2.13±1.8 (p=0.908)	0.50±0.3 (p=1.000)
Septoinferior	1.81±1.1 (p=0.252)	0.78±0.6 (p=0.075)
Septoanterior	0.90±0.4 (p=0.215)	0.55±0.5 (p=0.076)
Apex	2.26±0.9 (p=0.205)	1.50±1.1 (p=0.742)

consisted of 39 rings with a total of 24,336 lutetium oxyorthosilicate crystals of dimensions 4×4×25 mm covering an axial field-of-view (FOV) of 162 mm. The CT subsystem consisted of a 40-row ceramic detector with 1,344 channels per row and adaptive collimation. The z-sharp technique (a new approach used in STRATON x-ray tube technology allowing the doubling of resolution without reducing the detector element size) was used to acquire 64 slices per rotation with high temporal resolution [21].

Metallic leads

Phantom studies were performed to assess the impact of artefacts associated with metallic implants using a Kentrox RV 75 ICD lead and a Selox SR 60 pacemaker lead (Biotronik, Berlin, Germany). The ICD and pacemaker leads contained an electrode, a conductor wire and a battery. In addition, the ICD lead also had defibrillation electrodes (2.9 mm in diameter, 50 mm long) in the shock coils fabricated from a platinum/iridium alloy (80% Pt/20% Ir). The ICD lead consisted of two electrodes. The tip and ring electrodes were made of a platinum/iridium alloy (80% Pt/20% Ir). The tip of the pacemaker electrode was made of a 70% Pt/30% Ir alloy associated with a ring electrode made of an 80% Pt/20% Ir alloy. Both ICD and pacemaker leads comprised conductor wires used for connection of the

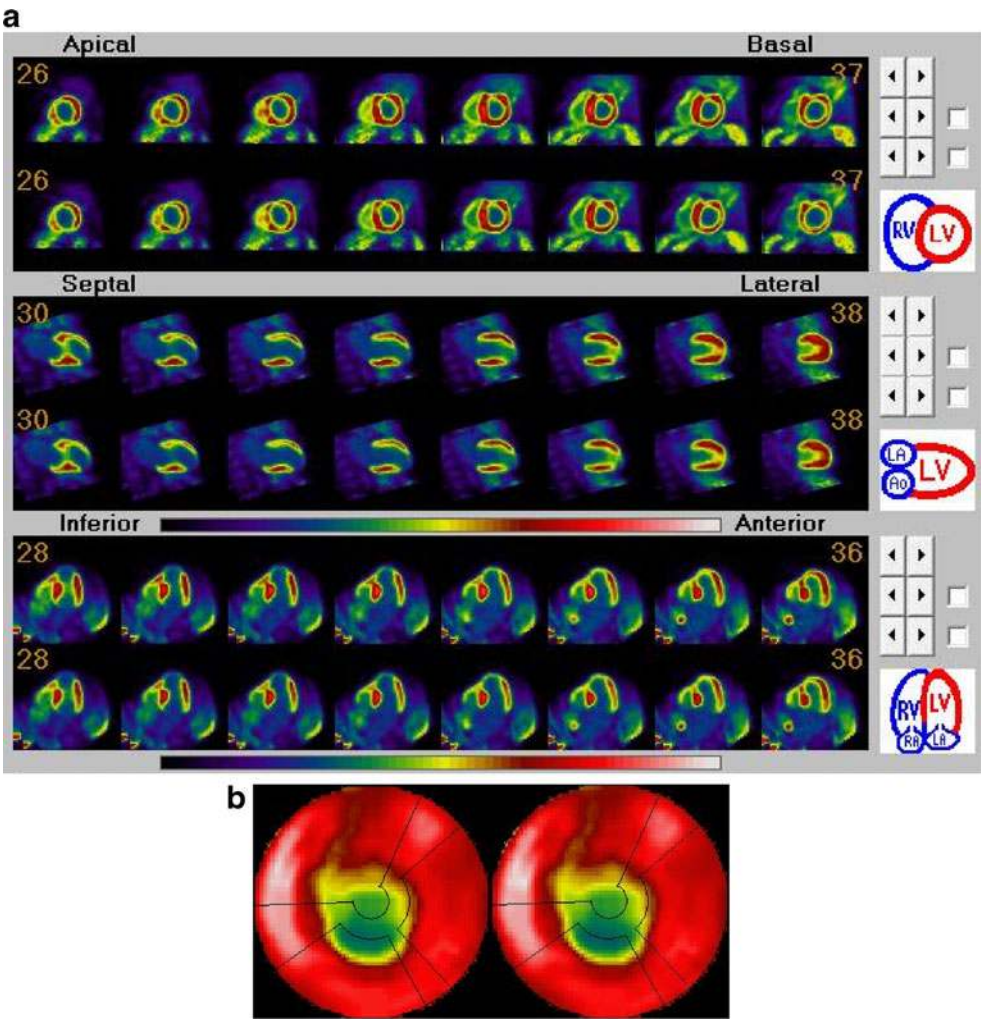

Fig. 5 **a** Typical short, vertical and horizontal long axis viability PET images in a patient with a pacemaker lead (*top rows* images corrected for attenuation with MAR, *bottom rows* images corrected for attenuation without MAR). **b** Bull's eye view of the viability study corrected for attenuation with MAR (*left*) and without MAR (*right*)

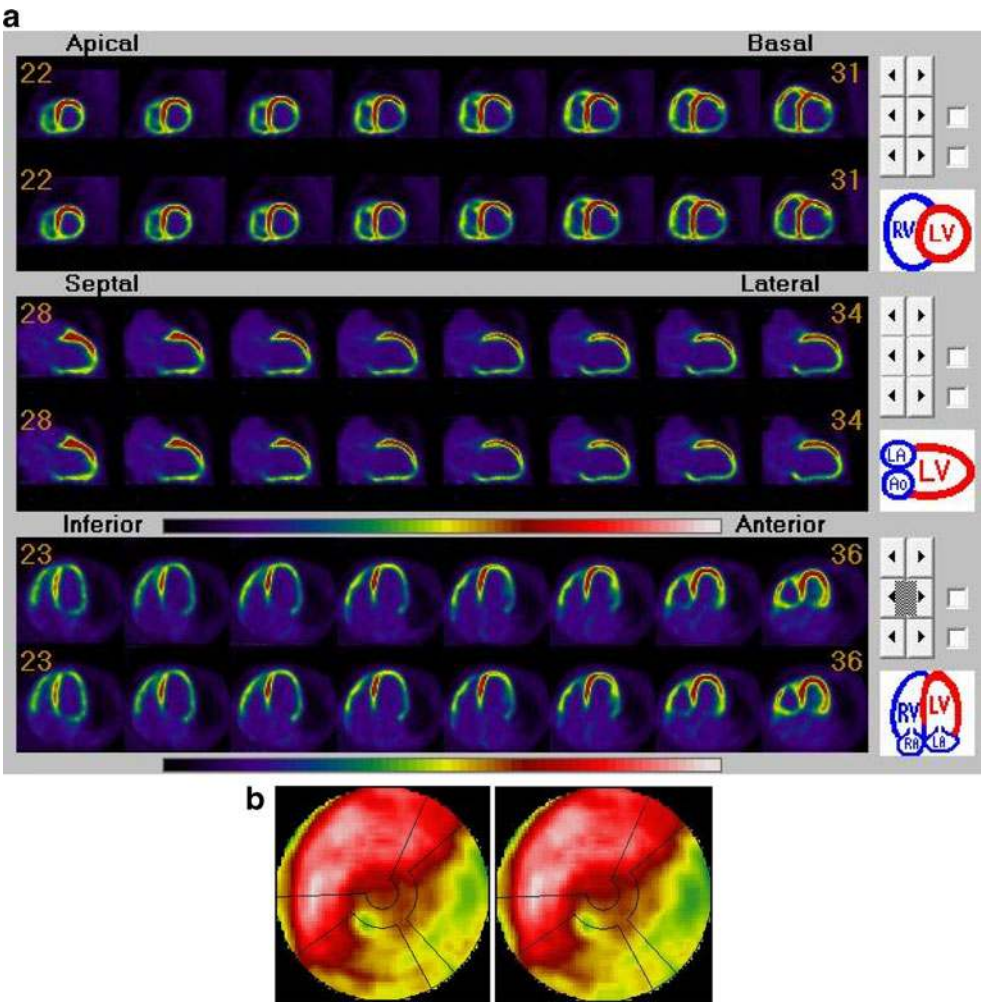

Fig. 6 **a** Typical short, vertical and horizontal long axis viability PET images in a patient with an ICD lead (*top rows* images corrected for attenuation with MAR, *bottom rows* images corrected for attenuation without MAR). **b** Bull's eye view of the viability study corrected for attenuation with MAR (*left*) and without MAR (*right*)

electrodes to the pacemaker or ICD batteries. The conductor wires used for tip and ring electrodes were made of MP35N (an alloy of Co, Cr and Ni), and the conductor wire for the shock coil was made of MP35N plus a 28% Ag core.

Phantom studies

Experimental phantom studies were conducted under controlled conditions to assess artefacts arising from metallic leads on PET/CT images. PET and CT images were perfectly registered without any misalignment artefact. The RSD thorax phantom (Radiology Support Devices, Long Beach, CA) and a phantom made in-house incorporating the heart of the RSD phantom hanging in a cylindrical water phantom were used (Fig. 1). The RSD thorax phantom is a fully tissue-equivalent anthropomorphic phantom including an anatomic heart model derived from patient data, ideal for evaluation of the detectability, extent and severity of myocardial infarcts in male and female patients. The heart model uses vacuum-formed shells designed using high-resolution contrast-enhanced ultrafast CT images of a normal subject slightly modified to facilitate its use. The volume of the heart chambers is 284 ml, while the volume of the myocardial wall is 240 ml.

The pacemaker and ICD leads were attached to the side of the right ventricle in both phantoms. The tips of the ICD and pacing leads were parallel to the axial FOV for worse-case assessment of the impact of metallic artefacts.

A total of 64.5 MBq of ^{18}F was injected into the RSD phantom 1 h prior to scanning, according to the following distribution in various individual organs: 43.5 MBq in the thorax cavity, 5.7 MBq in the myocardial wall, 1.2 and 1.7 MBq in the left and right lungs, respectively, and 12.4 MBq in the liver [22]. This corresponds to an activity concentration ratio of 1.4:6.4:1:1:3.4 in these organs, respectively. The activity injected into the heart phantom was 5.7 MBq in the myocardial wall and 32.8 MBq in the cylindrical part of the phantom for modelling the background in the vicinity of the heart (volume 6,180 ml). The phantoms were centred in the PET/CT scanners' FOV and the same protocol as that used for patient studies was used for data acquisition.

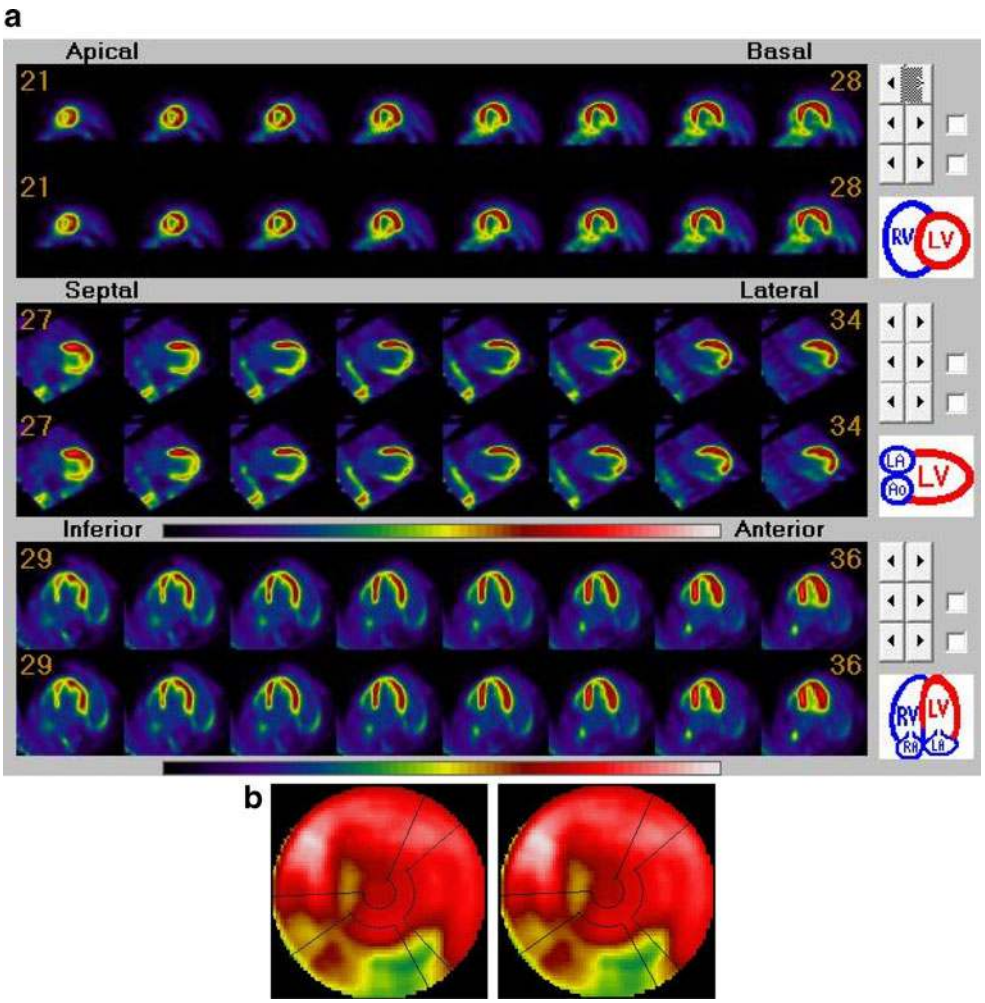

Fig. 7 **a** Typical short, vertical and horizontal long axis stress perfusion PET images in a patient with an ECG lead (*top rows* images corrected for attenuation with MAR, *bottom rows* images corrected for attenuation without MAR). **b** Bull's eye view of the perfusion study corrected for attenuation with MAR (*left*) and without MAR (*right*)

Clinical studies

Included in the study were 14 patients of whom eight underwent ^{13}N-ammonia (NH_3) perfusion and six ^{18}F-fluorodeoxyglucose (FDG) viability PET/CT examinations. The study population consisted of three groups: the first and second groups consisted of seven patients who had metallic implants (pacemaker and ICD leads) in their heart. The third group consisted of seven patients with significant metallic artefacts caused by ECG leads. All patients were in a supine position with arms behind the head, and underwent routine PET/CT scans with the protocols used in our department. ^{18}F-FDG PET/CT studies started with a low-dose CT scan (120 kVp, 74 effective mAs, 24×1.2 collimation, 0.45:1 pitch, and gantry rotation of 1 s per revolution) for attenuation correction with regular shallow breathing. PET data were then acquired for 10 min in list-mode format. Patients receiving the ^{13}N-ammonia perfusion examination underwent pharmacological intravenous dipyridamole stress testing followed by a similar low-dose CT scan as described above and stress PET data acquisition (12 min) in list-mode format. About 20 min later, PET rest data were acquired immediately after the second injection of 550 MBq of ^{13}N-ammonia following the second low-dose CT scan used for attenuation correction.

Image reconstruction

CT data were acquired using a free breathing protocol currently used for attenuation correction of PET datasets. The raw CT data were reconstructed using standard manufacturer-supplied software for the ACCT image (83 slices, 512×512 matrix, FOV 700 mm, slice thickness 3 mm, 2-mm increments). The 3-D PET list-mode data were first rebinned to 2-D sinograms and corrected for detector sensitivity, randoms, dead time, scatter and attenuation. An iterative reconstruction algorithm was applied (ordered-subset expectation maximization, OSEM, six iterations and eight subsets, with a 5-mm FWHM gaussian post-smoothing filter and a zoom factor of 2). As the goal of this study was to evaluate the above-mentioned MAR algorithm for CT-based attenuation correction of PET

Table 3 Mean relative differences in linear attenuation coefficients and activity values for all patients included in this study between images obtained without and with MAR (*patients 1–3* ICD leads, *patients 4–7* pacemaker leads, *patients 8–14* ECG leads). Although in some cases the differences are statistically significant, two expert clinicians did not report any clinically relevant differences

Patient no.	μ-map		PET	
	White region	Black region	White region	Black region
1	24.95±6.4 (p<0.001)	−2.94±1.4 (p<0.001)	13.25±2.1 (p<0.001)	6.73±3.4 (p<0.01)
2	19.93±5.6 (p<0.001)	−1.39±0.7 (p<0.005)	11.18±1.8 (p<0.001)	9.70±2.9 (p<0.001)
3	20.93±3.0 (p<0.001)	−1.46±1.0 (p<0.05)	12.30±3.5 (p<0.001)	12.06±.3 (p<0.001)
4	15.56±1.5 (p<0.001)	−0.19±0.1 (p<0.05)	7.71±1.0 (p<0.001)	11.16±2.8 (p<0.001)
5	9.98±1.7 (p<0.001)	−0.41±0.2 (p=0.712)	7.11±2.1 (p<0.001)	4.96±0.6 (p<0.001)
6	9.98±3.4 (p<0.001)	−0.25±0.2 (p=0.148)	6.83±1.5 (p<0.001)	5.32±1.6 (p<0.001)
7	16.47±3.5 (p<0.001)	−2.12±1.1 (p<0.005)	8.93±1.6 (p<0.001)	7.28±3.0 (p<0.01)
8	9.11±0.5 (p<0.001)	NA	0.55±0.12 (p<0.001)	NA
9	5.76±0.8 (p<0.001)	NA	0.96±0.21 (p<0.001)	NA
10	3.00±1.2 (p=0.294)	NA	0.84±0.56 (p<0.01)	NA
11	6.21±0.8 (p<0.001)	NA	0.49±0.25 (p<0.001)	NA
12	5.58±0.8 (p<0.005)	NA	0.38±0.13 (p<0.001)	NA
13	5.16±0.50 (p<0.01)	NA	0.41±0.18 (p<0.001)	NA
14	5.10±0.89 (p<0.01)	NA	0.56±0.16 (p<0.005)	NA

NA not applicable (black regions were not observed in ECG lead images due to the fact the leads were attached to the external part of body and only white artefacts were observed on the CT images).

images, the PET images were reconstructed twice, once using the standard manufacturer-supplied software currently used and once using the MAR algorithm as optionally available on the reconstruction toolbar of the Syngo software.

Assessment strategy

Images were subjected to qualitative and quantitative analysis to evaluate the impact of MAR in experimental phantoms and patients with metallic artefacts arising from pacemaker, ICD and ECG electrodes. Attenuation maps were generated using a MATLAB code (MathWorks, Natick, MA) developed in-house, and these were then forward-projected to produce attenuation correction factors. Quantitative analysis based on volumes of interest (VOI) was then performed using AMIDE image processing software [23]. About 40 VOIs were delineated on each pair of CT images obtained without and with MAR, followed by generation of linear regression plots from which Pearson correlation coefficients (R^2) and slopes were determined. VOI analysis was classified according to the location of the electrodes, white and black streak regions, and individual myocardial segments of the left ventricle. Mean attenuation coefficients and activity uptake estimates were obtained for both corrected and uncorrected μ-maps and reconstructed PET images.

PET images were also analysed using a 17-segment bull's eye view model for the left myocardium ventricle, with each region normalized to the maximum value. PET images were also reoriented along the short axis, horizontal and vertical long axis views to make clinical interpretation by two experienced physicians easier. For phantom studies, mean relative differences (bias) between actual and measured uptake values on PET images corrected for attenuation using CT images obtained without and with MAR were calculated. Activity uptakes in pairs of PET images were also compared using a two-sided paired t-test. Statistical analysis was performed using SPSS software, version 16 (SPSS, Chicago IL). Values of p less than 0.05 were considered statistically significant.

Results

Figure 2 shows a CT image and μ-map of the RSD phantom including both the pacemaker and ICD leads before and after applying the MAR algorithm. Although the metallic artefact was clear on CT images, it was much less clear on μ-maps particularly after applying the MAR algorithm. The artefact from the ICD leads was more pronounced because the metallic shock coil was larger than the pacemaker lead diameter. It is clear that MAR was more effective in reducing artefacts associated with ICD leads than those associated with pacemaker leads, as shown on difference images between μ-maps (Fig. 2).

Table 1 summarizes the results of VOI analysis for both μ-maps and PET images corresponding to ICD and

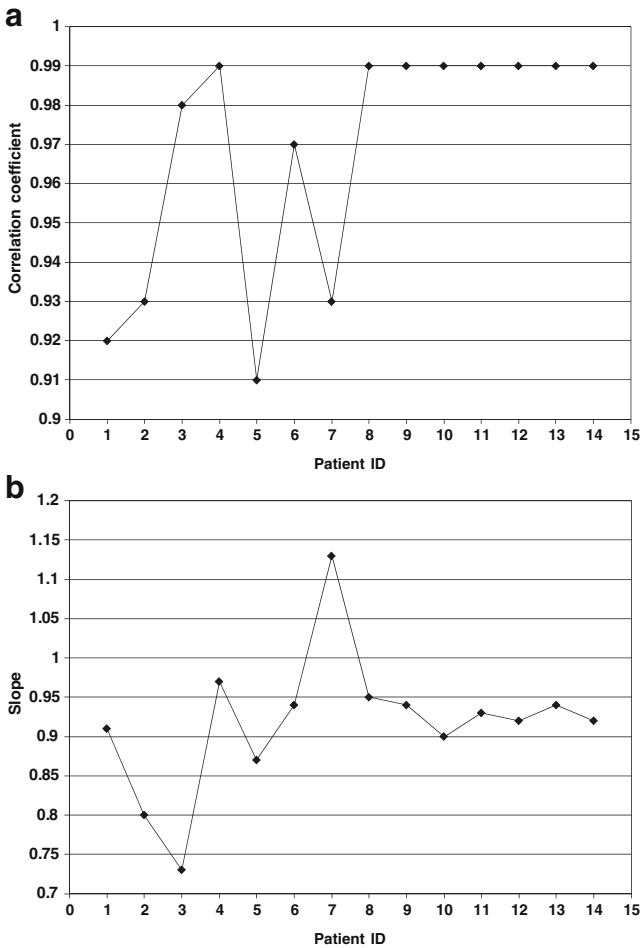

Fig. 8 Plots of correlation coefficients (**a**) and slopes of regression lines (**b**) resulting from the VOI-based analysis in the myocardial wall of PET images corrected for attenuation without and with MAR for patients with pacemaker, ICD and ECG leads (*patients 1–3* ICD leads, *patients 4–7* pacemaker leads, *patients 8–14* ECG leads; n=50, p<0.001)

pacemaker leads placed in the phantoms. The comparison is reported in two different artefactual regions including dark and white areas. Images reconstructed without and with MAR were compared. In addition, PET images obtained without and with MAR were compared with the actual activity in the phantom. The accuracy in PET tracer uptake quantification was improved more notably in the white regions. This was more pronounced for ICD leads owing to the higher attenuation of shock coils.

Figures 3 and 4 show CT images, μ-maps, PET and difference images of a transverse slice of a typical patient with pacemaker and ICD leads obtained with and without MAR. The influence of MAR can be seen in the difference images of both the μ-maps and PET images. The CT slice shown in Fig. 3 shows the slight metallic artefacts arising from pacemaker leads, while the shock coils in the ICD leads (Fig. 4) induced more intense metallic artefacts. The shock coil near the left ventricle resulted in more intense artefacts than the pacemaker leads and as such induced potent streak artefacts with artefactual regions showing increased and reduced activity uptake in some segments of the heart.

Table 2 lists the mean relative difference between uptake values from PET images corrected for attenuation without and with MAR based on bull's eye view analysis in patients with ICD and pacemaker leads. While there was no statistically significant difference in any segment of the myocardial wall between PET images obtained without and with MAR in the patients with a pacemaker, slightly elevated uptake was observed in some patients with ICD electrode leads in the lateroinferior, inferolateral, inferoseptal and apex regions since they are adjacent to the ICD electrode lead location in the left ventricle.

Figures 5, 6 and 7 show the short, vertical and horizontal long axis view PET images in addition to bull's eye view typical viability/perfusion patients with pacemaker, ICD and ECG leads reconstructed without and with MAR. It should be noted that we selected patients with strong metallic lead artefacts. However, PET images along standard cardiac axes did not exhibit any visible metallic artefacts especially for the pacemaker and ECG patient cohorts. Metallic artefacts were visible in the inferior and lateroinferior regions of bull's eye views in patients with an ICD lead owing to the vicinity of the ICD lead to the left ventricle in this special case. For patients with an ECG lead, no significant under/overestimation was observed between PET images corrected for attenuation without and with MAR. Likewise, the bull's eye view analysis confirmed the absence of statistically significant artefacts affecting the clinical diagnosis.

Table 3 shows the mean relative differences between generated μ-maps and attenuation-corrected PET images without and with MAR in both white and dark regions. ICD leads caused intense artefacts in both white and black regions in comparison with pacemaker and ECG leads.

The correlation coefficients and slopes of regression plots between PET images corrected for attenuation without and with MAR are illustrated in Fig. 8 for all patients. There was an excellent correlation between the mean uptake values in the myocardial wall between PET images corrected for attenuation without and with MAR, with higher correlations in patients with pacemaker and ECG leads.

Discussion

Metallic implants produce streak artefacts on CT images and therefore affect the generated μ-maps and attenuation-corrected PET images in PET/CT imaging [9, 24]. Since the

CT images are used for attenuation correction of the PET images in CTAC, the propagation of these artefacts to the PET images is the main concern. However, after applying down-sampling, smoothing and energy mapping, the amplitude of metallic artefacts usually declines. Nevertheless, depending on the amplitude and extension of these artefacts, they might introduce data inconsistencies thus resulting in inaccurate attenuation correction leading to overestimation of uptake values in related regions of PET images. Since photoelectric interactions are more significant at CT energies and are dependent on atomic number, the metallic composition of pacemaker and ICD electrodes can induce important artefacts on attenuation-corrected PET images. Central conductor wires and surgical clips with components with low atomic numbers do not produce noticeable artefacts on PET images [5].

In this study, we assessed the impact of MAR applied to CT images used for attenuation correction of PET data in cardiac PET/CT imaging with metallic objects arising from pacemakers, ICD and ECG leads. Tracer uptake was calculated in regions close to and far from the location of the metallic electrodes. In phantom studies, the mean relative differences between tracer uptake in heart segments without and with MAR were as much as 10.16±2.1 and 6.86±2.1 close to the metal and 4.43±0.5 and 2.98±0.5 in regions far from the metal of ICD and pacemaker leads, respectively.

PET images corrected for attenuation without MAR exhibited increased tracer uptake resulting from metallic artefacts corresponding to the location of the pacemaker and ICD leads in the right ventricle. This effect was greater in the lateroinferior, inferolateral and inferoseptal regions. This is in agreement with the observations of Goerres et al. [8, 24] and Kamel et al. [9] who found that PET artefacts arising from metallic materials in PET/CT oncological imaging were more pronounced near the metallic components. It would be expected that the magnitude and extension of metallic artefacts particularly in patients with ICD leads are correlated with the closeness of the ICD to the left ventricle [5], the number of leads used in the patients and the metal used for metallic components. Clearly patient movement, and respiratory and cardiac motion could also strengthen this effect.

The quantitative assessment of PET images corrected for attenuation without and with MAR through bull's eye view analysis confirmed that there were good correlations in the anterior wall in all patients. The mean relative differences between tracer uptake were greater in the lateroinferior wall than in the other regions for ICD leads than for pacemaker leads.

Qualitative assessment by experienced physicians and quantitative analysis demonstrated that there was no noticeable difference between PET images corrected for attenuation without and with MAR in the case of pacemaker leads. This is in agreement with the observations of DiFilippo and Brunken [5]. The corresponding evaluation of the patients with an ICD revealed little increase in tracer uptake in the inferior wall in relation to the ICD electrode location and this did not induce any erroneous clinical interpretation by two observers. In the patients with an ECG with high streak artefacts caused by the ECG electrodes, although the MAR method corrected the μ-map in regions contaminated with artefacts, the observers did not report any difference between PET images corrected for attenuation without and with MAR. Furthermore, the MAR method resulted in enhanced recovery for white streak artefacts in comparison with dark streak artefacts.

While this study showed that MAR can reduce the metallic artefacts in the generated μ-map, the resulting artefacts as propagated onto PET images by the attenuation correction process did not induce erroneous interpretation of the PET images. In some patients with ICD leads, depending on the location of the shock coils and electrodes, there were some variations in the inferior and apex segments. In these patients, the MAR method produced improved results in related regions. Future efforts will be directed towards expanding the number of patient examinations by utilizing a large pool of clinical datasets to increase the statistical power.

Conclusion

The effectiveness of MAR on CT images used for attenuation correction to improve cardiac PET images was assessed in both phantom and clinical studies. Although MAR was able to effectively improve the quality of the generated μ-maps and reduce the magnitude of metallic artefacts, it had no effect on the clinical interpretation of PET images. One can thus argue that cardiac PET images reconstructed using CT-based attenuation correction in the presence of metallic leads can be reported with confidence without correcting the CT images for metallic artefacts. It should be emphasized, however, that in some specific cases with multiple ICD leads attached to the myocardial wall, MAR may still be useful for accurate attenuation correction. Another important feature of the MAR algorithm is the substantial reduction in streak artefacts on CT images that could be exploited to improve their diagnostic value.

Acknowledgments This work was supported by Shahid Behshti University and Research Center for Science and Technology in Medicine, Tehran University of Medical Sciences, and the Swiss National Science Foundation (grant no. 31003A-125246). The authors would like to thank Mr. Mohammad Hossin Farhani for providing the software used for image processing and Biotronik (Geneva) for providing the ICD and pacemaker leads.

Conflicts of interest None.

References

1. Zaidi H, Montandon M-L, Alavi A. Advances in attenuation correction techniques in PET. PET Clin 2007;2:191–217.
2. Souvatzoglou M, Bengel F, Busch R, Kruschke C, Fernolendt H, Lee D, et al. Attenuation correction in cardiac PET/CT with three different CT protocols: a comparison with conventional PET. Eur J Nucl Med Mol Imaging 2007;34:1991–2000.
3. Di Carli MF, Dorbala S, Meserve J, El Fakhri G, Sitek A, Moore SC. Clinical myocardial perfusion PET/CT. J Nucl Med 2007;48:783–93.
4. Halpern BS, Dahlbom M, Waldherr C, Yap CS, Schiepers C, Silverman DH, et al. Cardiac pacemakers and central venous lines can induce focal artifacts on CT-corrected PET images. J Nucl Med 2004;45:290–3.
5. DiFilippo FP, Brunken RC. Do implanted pacemaker leads and ICD leads cause metal-related artifact in cardiac PET/CT? J Nucl Med 2005;46:436–43.
6. Ay M, Zaidi H. Assessment of errors caused by x-ray scatter and use of contrast medium when using CT-based attenuation correction in PET. Eur J Nucl Med Mol Imaging 2006;33:1301–13.
7. Buther F, Stegger L, Dawood M, Range F, Schafers M, Fischbach R, et al. Effective methods to correct contrast agent-induced errors in PET quantification in cardiac PET/CT. J Nucl Med 2007;48:1060–8.
8. Goerres GW, Ziegler SI, Burger C, Berthold T, Von Schulthess GK, Buck A. Artifacts at PET and PET/CT caused by metallic hip prosthetic material. Radiology 2003;226:577–84.
9. Kamel EM, Burger C, Buck A, von Schulthess GK, Goerres GW. Impact of metallic dental implants on CT-based attenuation correction in a combined PET/CT scanner. Eur Radiol 2003;13:724–8.
10. Lemmens C, Montandon M-L, Nuyts J, Ratib O, Dupont P, Zaidi H. Impact of metal artefacts due to EEG electrodes in brain PET/CT imaging. Phys Med Biol 2008;53:4417–29.
11. Abdoli M, Ay MR, Ahmadian A, Zaidi H. A virtual sinogram method to reduce dental metallic implant artefacts in computed tomography-based attenuation correction for PET. Nucl Med Commun 2010;31:22–31.
12. Martinez-Möller A, Souvatzoglou M, Navab N, Schwaiger M, Nekolla SG. Artifacts from misaligned CT in cardiac perfusion PET/CT studies: frequency, effects, and potential solutions. J Nucl Med 2007;48:188–93.
13. Lautamaki R, Brown T, Merrill J, Bengel F. CT-based attenuation correction in 82Rb-myocardial perfusion PET/CT: incidence of misalignment and effect on regional tracer distribution. Eur J Nucl Med Mol Imaging 2008;35:305–10.
14. Gould KL, Pan T, Loghin C, Johnson NP, Guha A, Sdringola S. Frequent diagnostic errors in cardiac PET/CT due to misregistration of CT attenuation and emission PET images: a definitive analysis of causes, consequences, and corrections. J Nucl Med 2007;48:1112–21.
15. Schuster DM, Halkar RK, Esteves FP, Garcia EV, Cooke CD, Syed MA, et al. Investigation of emission-transmission misalignment artifacts on rubidium-82 cardiac PET with adenosine pharmacologic stress. Mol Imaging Biol 2008;10:201–8.
16. Bazalova M, Beaulieu L, Palefsky S, Verhaegen F. Correction of CT artifacts and its influence on Monte Carlo dose calculations. Med Phys 2007;34:2119–32.
17. Yazdi M, Gingras L, Beaulieu L. An adaptive approach to metal artifact reduction in helical computed tomography for radiation therapy treatment planning: experimental and clinical studies. Int J Radiat Oncol Biol Phys 2005;62:1224–31.
18. Hamill JJ, Brunken RC, Bybel B, DiFilippo FP, Faul DD. A knowledge-based method for reducing attenuation artefacts caused by cardiac appliances in myocardial PET/CT. Phys Med Biol 2006;51:2901–18.
19. Kennedy JA, Israel O, Frenkel A, Bar-Shalom R, Azhari H. The reduction of artifacts due to metal hip implants in CT-attenuation corrected PET images from hybrid PET/CT scanners. Med Biol Eng Comput 2007;45:553–62.
20. Mirzaei S, Guerchaft M, Bonnier C, Knoll P, Doat M, Braeutigam P. Use of segmented CT transmission map to avoid metal artifacts in PET images by a PET-CT device. BMC Nucl Med 2005;5:3.
21. Flohr TG, Stierstorer K, Ulzheimer S, Bruder H, Primak AN, McCollough CH. Image reconstruction and image quality evaluation for a 64-slice CT scanner with z-flying focal spot. Med Phys 2005;32:2536–47.
22. Zasadny KR, Wahl RL. Standardized uptake values of normal tissues at PET with 2-[fluorine-18]-fluoro-2-deoxy-D-glucose: variations with body weight and a method for correction. Radiology 1993;189:847–50.
23. Loening AM, Gambhir SS. AMIDE: a free software tool for multimodality medical image analysis. Mol Imaging 2003;2:131–7.
24. Goerres GW, Hany TF, Kamel E, von Schulthess GK, Buck A. Head and neck imaging with PET and PET/CT: artefacts from dental metallic implants. Eur J Nucl Med Mol Imaging 2002;29:367–70.